

Double rotatory power reversal and continuous Kerr angle in bi-isotropic media with anomalous Hall current

Alex Q. Costa^{a,*}, Pedro D. S. Silva^{a,b,†} and Manoel M. Ferreira Jr.^{a,c,‡}

^aPrograma de Pós-graduação em Física, Universidade Federal do Maranhão,
Campus Universitário do Bacanga, São Luís, Maranhão 65080-805, Brazil

^bCoordenação do Curso de Ciências Naturais - Física, Universidade Federal do Maranhão,
Campus de Bacabal, Bacabal, Maranhão, 65700-000, Brazil and

^cDepartamento de Física, Universidade Federal do Maranhão,
Campus Universitário do Bacanga, São Luís, Maranhão 65080-805, Brazil

We investigate optical properties of bi-isotropic materials under the anomalous Hall effect (AHE) of the axion electrodynamics. Four refractive indices associated with circularly polarized waves are achieved, implying circular birefringence with rotatory power (RP) endowed with double sign reversal, an exotic optical signature for chiral dielectrics. The Kerr rotation and ellipticity are analyzed, with an unusual observation of rotation angle deprived of discontinuity. Anomalous reflection (greater than unity) is also reported, associated with negative refraction stemming from the anomalous transport properties. These effects constitute the singular optical signature of bi-isotropic media with the AHE.

Introduction. Optical characterization of chiral media constitutes a powerful technique for matter characterization. Birefringence appears as a key feature of optically active media, being measured by the rotatory power (RP) [1], which finds application in the description of bi-isotropic matter [2, 3], organic compounds [4], and chiral metamaterials [5]. The dispersive RP can be anomalous if it undergoes reversion with the frequency [6]. The Kerr rotation angles provide magneto-optical signatures of reflected light [7, 8]. The magneto-optic Kerr effect (MOKE) and magneto-optical effects in complex materials are broadly employed to probe properties of topological insulators [9], new graphene composites [10] and to examine giant Kerr rotation in Weyl semimetals [11] and time-reversal broken systems [12].

Nonconventional phenomena, such as the Chiral Magnetic Effect (CME), where an electric current is generated along an applied magnetic field due to an imbalance in the number density of chiral fermions with opposite handedness [13, 14], has played an important role in Weyl metals [15] and semimetals [16, 17]. Another relevant quantum-anomaly induced transport phenomenon is the anomalous Hall effect (AHE), due to the separation of Weyl nodes in momentum for right- and left-handed fermions. The AHE and the CME can be effectively described by including the axion term [18–21], $\mathcal{L} = \theta(\mathbf{E} \cdot \mathbf{B})$, in the classical Maxwell Lagrangian in continuous matter, where the anomalous Hall current takes place, $\nabla \theta \times \mathbf{E}$. For the special case of a nondynamical axion field, $\partial_t \theta = cte$, $\nabla \theta = cte$, one recovers the Maxwell-Carroll-Field-Jackiw (MCFJ) electrodynamics [22] in continuous matter [23, 24]. For a time-independent axion field, $\partial_t \theta = 0$, the Ampere's law reads $\nabla \times \mathbf{H} - \partial_t \mathbf{D} = \mathbf{J} + \mathbf{b} \times \mathbf{E}$, with $\mathbf{b} = \nabla \theta$ standing

for the axion field gradient. The axion electrodynamics effectively describes relevant aspects of Weyl semimetals [25], optical properties of exotic metamaterials [26], axion dielectrics [27, 28], connections with the London equation and Weyl semimetals [29, 30], and optical reflection properties at the surface of an axion dielectric [31]. Wave propagation in bi-isotropic media endowed with the axion magnetic current term was classically addressed as well, yielding dispersive birefringence and rotatory power endowed with sign reversal [32], a typical property of rotating plasmas [33], chiral plasmas [34], graphene systems [35], and particular Weyl semimetals [36]. Investigations on reflection for normal incidence at a Weyl semimetal surface have yielded anomalous reflectance (greater than unity) due to chiral magnetic instabilities associated with CME and AHE axion terms [37, 38]. Moreover, nonreciprocal thermal radiation emission in Weyl semimetals (with AHE) has shown negative emissivity at low frequencies, deviating from Planck's law [39]. Kerr rotation and ellipticity angles [40] depending on the frequency were reported in Weyl semimetals [41], where it can be used to design circular polarizers or optical isolators [42, 43].

In this letter, we investigate the optical characterization of bi-isotropic media endowed with the AHE, including circular birefringence, Kerr rotation, Kerr ellipticity, and anomalous reflection, achieving new remarkable features that compose a specific optical signature of such a system. Throughout this work, we use natural units.

Dispersion relations and refractive indices. In the plane wave ansatz, one writes the Maxwell equations modified by the AHE term,

$$\mathbf{k} \cdot \mathbf{D} = -\mathbf{b} \cdot \mathbf{B}, \quad \mathbf{k} \times \mathbf{H} = -\omega \mathbf{D} + i \mathbf{b} \times \mathbf{E}, \quad (1)$$

which must be considered with the linear bi-isotropic constitutive relations

$$\mathbf{D} = \epsilon \mathbf{E} + \alpha \mathbf{B}, \quad \mathbf{H} = \frac{1}{\mu} \mathbf{B} + \beta \mathbf{E}, \quad (2)$$

* costa.alex@discente.ufma.br, prof.costalex@gmail.com

† pedro.dss@ufma.br, pdiego.10@hotmail.com

‡ manoeljr.ufma@gmail.com, manoel.messias@ufma.br

where α and β are complex coefficients that fulfill the condition $\beta^* = -\alpha$ to assure energy conservation. Manipulating the Maxwell equations and Eq. (2), one finds the equation $M_{ij}E^j = 0$, with $M_{ij} = n^2\delta_{ij} - n_in_j - \mu\epsilon_{ij}$, and the effective electric permittivity tensor,

$$\bar{\epsilon}_{ij}(\omega) = \epsilon\delta_{ij} + \frac{1}{\omega}(\alpha + \beta)\epsilon_{ilj}k^l - \frac{i}{\omega}\epsilon_{ilj}b^l, \quad (3)$$

which includes the magnetoelectric and the AHE contributions. Here, n_i is a refractive index component, $\mathbf{n} = \mathbf{k}/\omega$. Solving $\det[M_{ij}] = 0$ provides the refractive indices

$$n_{RCP,\pm} = \mu\alpha'' \pm Q_-, \quad n_{LCP,\pm} = -\mu\alpha'' \pm Q_+, \quad (4)$$

$$Q_{\pm} = \sqrt{\mu\epsilon + \mu^2\alpha''^2 \pm \mu b/\omega}. \quad (5)$$

where \mathbf{n} is considered parallel to the vector \mathbf{b} , and $\alpha + \beta = 2i\alpha''$, with $\text{Im}[\alpha] = \alpha''$. The indices $n_{RCP,\pm}$ and $n_{LCP,\pm}$ are associated with right-handed circularly polarized (RCP) mode and left-handed circularly polarized (LCP) wave, respectively, given by $\hat{\mathbf{e}}_{RCP,LCP} = \hat{\mathbf{x}} \mp i\hat{\mathbf{y}}$.

The indices $n_{RCP,\pm}$ are complex in the frequency window $\omega < \omega_0$, with

$$\omega_0 = b/(\epsilon + \alpha''^2\mu), \quad (6)$$

being $0 < \omega < \omega_0$ the absorption zone (for positive definite electromagnetic parameters). In Fig. 1, we illustrate the frequency behavior of the indices $n_{RCP,\pm}$ of Eq. (4). For $\omega > \omega_0$, the indices become real, being $n_{RCP,+}$ (red line) positive and monotonically increasing (normal dispersion), while $n_{RCP,-}$ (blue line) is progressively decreasing (anomalous dispersion).

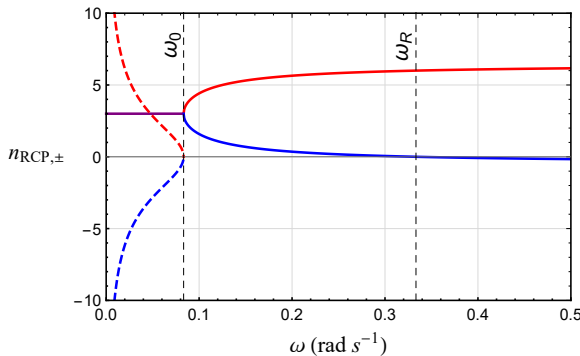


FIG. 1. Refractive indices $n_{RCP,\pm}$ of Eq. (4). The red (blue) lines represent $n_{RCP,+}$ ($n_{RCP,-}$). The solid (dashed) line indicates the real (imaginary) part of the refractive indices. The solid purple line represents the real parts of $n_{RCP,+}$ and $n_{RCP,-}$, lying on top of each other. Here, we have used $\mu = 1, \epsilon = 3, \alpha'' = 3$ and $b = 1 \text{ s}^{-1}$.

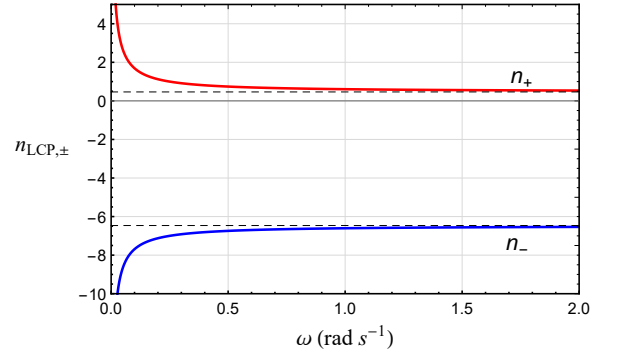


FIG. 2. Refractive indices $n_{LCP,\pm}$ of Eq. (4). The red (blue) line indicates the positive (negative) refractive index ($n_{LCP,\pm}$), respectively. The horizontal dashed lines are given by Eq. (7). Here, we have used $\mu = 1, \epsilon = 3, \alpha'' = 3$ and $b = 1 \text{ s}^{-1}$.

Furthermore, the index $n_{RCP,-}$ becomes negative for $\omega > \omega_R$ with $\omega_R = b/\epsilon$, as shown in Fig. 1. As for the LCP modes, the associated refractive indices, $n_{LCP,\pm}$, are both real, being $n_{LCP,-}$ negative for any frequency, while $n_{LCP,+}$ is always positive, as shown in Fig. 2. In the high-frequency regime, the indices $n_{LCP,\pm}$ and $n_{RCP,\pm}$ tend to positive and negative asymptotic values,

$$n_{LCP,\pm}|_{\text{high}} = -\mu\alpha'' \pm \sqrt{\mu\epsilon + \mu^2\alpha''^2}, \quad (7)$$

$$n_{RCP,\pm}|_{\text{high}} = \mu\alpha'' \pm \sqrt{\mu\epsilon + \mu^2\alpha''^2}, \quad (8)$$

which represent the frequency-independent indices of a bi-isotropic dielectric.

Birefringence and Rotatory Power. The circular birefringence is measured in terms of the rotatory power,

$$\delta_{RP} = -\frac{\omega}{2} [\text{Re}(n_{LCP,\pm}) - \text{Re}(n_{RCP,\pm})]. \quad (9)$$

The fact that we have two refractive indices for each propagating wave indicates that we have the possibility of four distinct results for the rotatory power, given as follows:

$$\delta_{+,\pm} = \frac{\omega}{2} \text{Re}(2\mu\alpha'' - Q_+ \pm Q_-), \quad (10)$$

$$\delta_{-,\pm} = \frac{\omega}{2} \text{Re}(2\mu\alpha'' + Q_+ \pm Q_-), \quad (11)$$

One notes that Q_- contributes only when it is real, that is, for $\omega > \omega_0$, with ω_0 given by Eq. (6). The behavior of the rotatory power $\delta_{+,\pm}$ of Eq. (10) as a function of the frequency can be observed in Fig. 3, being both equal in the range $0 < \omega < \omega_0$ (see the purple line), where they receive contribution only of the first root (Q_+). In this frequency range, both RPs $\delta_{+,\pm}$ possess sign reversal at $\omega = \omega'$, with ω' given by $\omega' = b/(3\mu\alpha''^2 - \epsilon)$.

For $\omega > \omega_0$, the RPs begin to receive the contribution of the second root, resulting in the splitting starting at $\omega = \omega_0$, from which $\delta_{+,+}$ exhibits an increasing behavior (see the red line), while $\delta_{+,-}$ has decreasing magnitude (see the blue line). Along with that, the RP $\delta_{+,-}$ exhibits a second (additional) sign reversal at the frequency,

$\omega'' = b/(2\alpha''\sqrt{\mu\epsilon})$, with $\omega'' > \omega_0$. This double sign inversion is an effect of both the magnetoelectric and AHE parameters, a very unusual feature that may work as an optical signature of this chiral system. A single RP reversion was reported for the case of a bi-isotropic dielectric in the presence of an isotropic axion magnetic current [32]. For high-frequencies, where the term b/ω becomes negligible, the coefficients $\delta_{+,+}$ and $\delta_{+,-}$ recover a linear behavior with a positive (negative) slope.

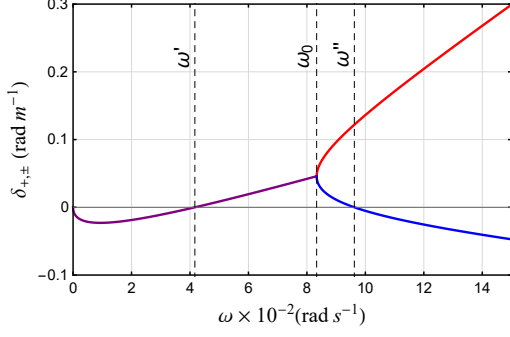


FIG. 3. Rotatory power $\delta_{+,±}$ of Eq. (10), constructed using the two refractive indices for the RCP wave and $n_{LCP,+}$. The RP $\delta_{+,+}$ is depicted by the purple-red line, while $\delta_{+,-}$ is demarcated by the purple-blue line, endowed with double sign reversal. Here, we have used $\mu = 1, \epsilon = \alpha'' = 3$, and $b = 1 \text{ s}^{-1}$.

Kerr rotation and Kerr ellipticity. Considering incident light stemming from medium 1 (a usual dielectric described by permittivity ϵ_1 and permeability μ_1) and reflecting on the surface of medium 2 (a chiral dielectric described by the parameters ϵ, μ , the axion vector \mathbf{b} , and the refractive indices of Eq. (4)), we obtain two Fresnel coefficients for each left-handed circularly polarized (LCP) mode and right-handed circularly polarized (RCP) wave at normal incidence, namely

$$r_{LCP,\pm} = \frac{\mu_1 n_{LCP,\pm} - \mu n_1}{\mu_1 n_{LCP,\pm} + \mu n_1}, \quad (12a)$$

$$r_{RCP,\pm} = \frac{\mu_1 n_{RCP,\pm} - \mu n_1}{\mu_1 n_{RCP,\pm} + \mu n_1}. \quad (12b)$$

The latter can be used to define the Kerr angle expression

$$\Delta_{\pm,\pm} = \left(\frac{r_{LCP,\pm} - r_{RCP,\pm}}{r_{LCP,\pm} + r_{RCP,\pm}} \right), \quad (13)$$

where the first (second) \pm subscript is related to $n_{LCP,\pm}$ ($n_{RCP,\pm}$). The elements $\Delta_{\pm,\pm}$ are generally complex,

$$\Delta_{\pm,\pm} = \Delta'_{\pm,\pm} + i\Delta''_{\pm,\pm}, \quad (14)$$

with $\Delta'_{\pm,\pm} = \text{Re}[\Delta_{\pm,\pm}]$ and $\Delta''_{\pm,\pm} = \text{Im}[\Delta_{\pm,\pm}]$. The real and imaginary parts provide the Kerr angles (ellipticity

and rotation) [8, 31], respectively,

$$\tan(2\theta_K^{\pm,\pm}) = -\frac{2\Delta''_{\pm,\pm}}{1 - |\Delta_{\pm,\pm}|^2}, \quad (15)$$

$$\sin(2\eta_K^{\pm,\pm}) = \frac{2\Delta'_{\pm,\pm}}{1 + |\Delta_{\pm,\pm}|^2}. \quad (16)$$

Recalling the refractive indices in Eq. (4), we note that $n_{LCP,+}$ and $n_{RCP,+}$ are connected to the usual refraction. On the other hand, the indices $n_{LCP,-}$ and $n_{RCP,-}$ (for $\omega > \omega_R$) are related to negative refraction. Thus, the element $\Delta_{+,+}$ provides the Kerr angles for the usual refraction case, $\Delta_{-,-}$ yields the Kerr angles for the pure negative refraction scenario, and $\Delta_{\pm,\mp}$ are associated with mixing effects of normal and negative refraction.

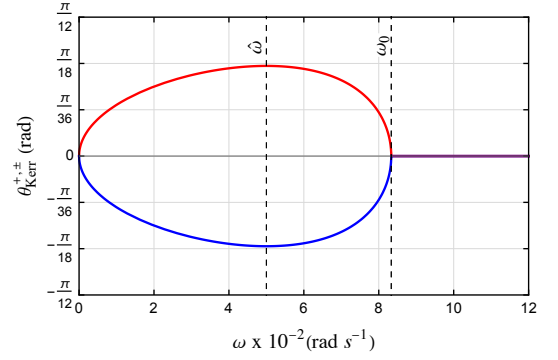


FIG. 4. Kerr rotation $\theta_K^{\pm,\pm}$ of Eq. (15). The red line shows the behavior of $\theta_K^{+,+}$, composed by the indices $n_{LCP,+}$ and $n_{RCP,+}$. The blue line depicts $\theta_K^{+,-}$, constituted with $n_{LCP,+}$ and $n_{RCP,-}$. The purple line is defined for the region where both $\theta_K^{\pm,\pm}$ are null. Here, we have used $n_1 = 1, \mu_1 = 1, \mu = 1, \epsilon = 3, \alpha'' = 3$, and $b = 1 \text{ s}^{-1}$.

As previously discussed, absorption occurs only in the range $\omega < \omega_0$, being associated with RCP refractive indices. Thus, only in this frequency interval, one finds $\Delta'' \neq 0$, providing a non-null Kerr rotation for the reflected wave. In the following subsection, we examine the Kerr rotation angles for $\Delta_{+,\pm}$ and $\Delta_{-,\pm}$ in terms of frequency.

The general behaviors of $\theta_K^{\pm,\pm}$ in terms of the frequency are illustrated in Fig. 4. We observe that the factors $\theta_{Kerr}^{+,+}$ and $\theta_K^{+,-}$ are positive and negative, respectively, meaning that the polarization ellipse of the reflected wave is rotated in the counterclockwise (clockwise) direction relative to x -axis of polarization basis [45].

The continuous Kerr rotation angle of Fig. 4 is a remarkable peculiar characteristic of this bi-isotropic system endowed with AHE term, in contrast to the usual discontinuous Kerr rotation angles that occur in media ruled by the axion electrodynamics [11]. For the dielectric system here considered, such a discontinuity takes place only when

$$n_1 > \mu_1 \alpha'', \quad (17)$$

for which the squared magnitude of coefficient $\Delta_{+,+}$ becomes equal to unity, leading to a divergence for the Kerr rotation angle tangent ($\theta_K = \pi/4$). The latter manifests itself as an abrupt sign change (discontinuity) in $\theta_{Kerr}^{+,+}$ at the frequency $\tilde{\omega}$ given by $\tilde{\omega} = \mu_1^2 b / (\mu_1^2 \epsilon + \mu n_1^2)$. Figure 5 illustrates the frequency behavior of $\theta_{Kerr}^{+,+}$ under condition (17). Notice that at the frequencies $\tilde{\omega}_1$ and $\tilde{\omega}_2$ for the red (blue) line, respectively, the rotation of the polarization ellipse changes abruptly, indicating a reversal in the ellipse polarization rotation.

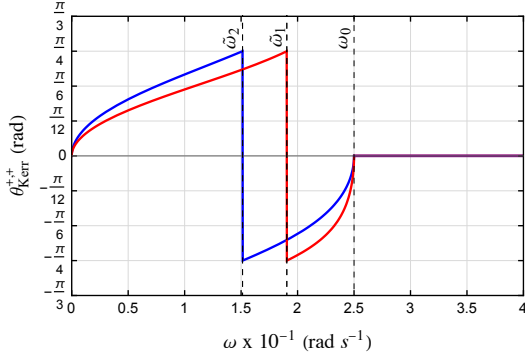


FIG. 5. Kerr rotation $\theta_K^{+,+}$ of Eq. (15) under the condition (17). The red and blue lines show $\theta_K^{+,+}$ (obtained by using $n_{LCP,+}$ and $n_{RCP,+}$) for $n_1 = 1.5$ and $n_1 = 1.9$, respectively. The purple line indicates $\theta_K^{+,+} = 0$. Here, we have used $\mu_1 = 1$, $\mu = 1$, $\epsilon = 3$, $\alpha'' = 1$, $b = 1 \text{ s}^{-1}$, $n_1 = 1.5$ (red), and $n_1 = 1.9$ (blue).

The other Kerr rotation angles, $\theta_K^{-,\pm}$, which are obtained by using $n_{LCP,-}$, can be easily found by implementing $\Delta_{-,\pm} = \Delta_{+,\pm}|_{Q_+ \rightarrow -Q_+}$, and will not be addressed here.

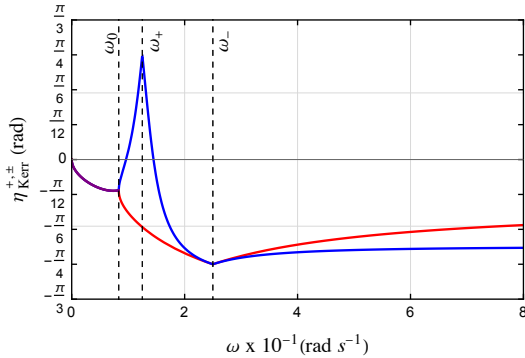


FIG. 6. Kerr ellipticity $\eta_K^{+,+}$ of Eq. (16). The red line shows $\eta_K^{+,+}$, while the blue curve depicts $\eta_K^{+,-}$. The purple line indicates the region both $\eta_K^{+,+}$ are equal to each other. Here, we have used $n_1 = 1$, $\mu_1 = 1$, $\mu = 1$, $\epsilon = 3$, $\alpha'' = 3$, and $b = 1 \text{ s}^{-1}$. When $\eta_K = 0$, the reflected wave is linearly polarized. The extreme values ($\pm\pi/4$) are associated with left- and right-handed circularly polarized waves.

Kerr ellipticity angles $\eta_K^{\pm,\pm}$. The Kerr ellipticities, given by Eq. (16), are non-null for any frequency since

the refractive indices (4) possess at least one real piece. For $0 < \omega < \omega_0$, it holds $\text{Re}[n_{RCP,\pm}] = \mu\alpha''$, so that the four initial possibilities of Eq. (16) are reduced to only two, in accordance with the double sign of $n_{LCP,\pm}$. For the index $n_{LCP,+}$, we define $\eta_K^{+,\pm}$, whose behavior in terms of frequency is illustrated in Fig. 6. For $\omega < \omega_0$, one has $\eta_K^{+,+} = \eta_K^{+,-}$, as already explained, behavior represented by the purple line in Fig. 6. In the frequencies ω_{\pm} , given by

$$\omega_{\pm} = \frac{\mu_1 b}{2\mu\alpha'' \sqrt{\mu_1 \epsilon_1} \pm (\mu_1 \epsilon - \mu \epsilon_1)}. \quad (18)$$

the ellipticity is $\pm\pi/4$, respectively, where the wave is circularly polarized. In the range $\omega > \omega_0$, the indices $n_{RCP,\pm}$ are real, assuming two different values, therefore making $\eta_K^{+,+} \neq \eta_K^{+,-}$, splitting the Kerr ellipticity into two distinct lines (red and blue) in Fig. 6.

Moreover, the Kerr ellipticity $\eta^{+,-}$ presents a double reversion sign, indicating that the reflected wave can be turned into linearly polarized mode ($\eta^{+,-} = 0$) at two distinct frequencies. This peculiar aspect seems to be in agreement with the double rotatory power reversal observed for $\delta_{+,-}$ in Fig. 3.

Reflectance and super reflectance effect. Recently, anomalous reflection ($R > 1$), at normal incidence, has been reported as one key feature of Weyl semimetals in the presence of both axion terms (b_0 and \mathbf{b}) [38]. Here, we report that a similar effect can appear in bi-isotropic media modified by the AHE term. Starting from the Fresnel coefficients (12a) and (12b), one obtains the reflection coefficients,

$$R_{LCP}^{\pm} = \left| \frac{\mu_1 (\mu\alpha'' \mp Q_+) + \mu n_1}{\mu_1 (\mu\alpha'' \mp Q_+) - \mu n_1} \right|^2, \quad (19a)$$

$$R_{RCP}^{\pm} = \left| \frac{\mu_1 (\mu\alpha'' \pm Q_-) - \mu n_1}{\mu_1 (\mu\alpha'' \pm Q_-) + \mu n_1} \right|^2, \quad (19b)$$

where Q_{\pm} are given in Eqs. (5). We then address the two reflection amplitudes, R_{LCP}^- and R_{RCP}^- , stemming from $n_{LCP,-}$ (always negative for all frequencies) and $n_{RCP,-}$ (with negative real part for $\omega > \omega_R$). In Fig. 7, we illustrate reflectances that exhibit anomalous behaviors. As for R_{RCP}^- (red line), it initially decreases with frequency, reaches a null value near ω_0 , and then augments monotonically, becoming greater than unity for $\omega > \omega_R$, which is exactly the frequency whereupon the refractive index $n_{RCP,-}$ becomes negative.

On the other hand, the coefficient R_{LCP}^- (blue line) already starts at unit, $R_{LCP}^- = 1$, and progressively enlarges with the frequency, defining an increasing anomalous reflectance (R greater than unit) for the entire frequency domain. Both R_{LCP}^- and R_{RCP}^- are endowed with super reflectance, being this property associated with negative refraction, a hallmark of metamaterials [5, 44]. The negative refraction of the indices n_{RCP}^- and n_{LCP}^- occurs as a consequence of an anomalous increasing wave magnitude that propagates along the direction $-\hat{z}$ [38].

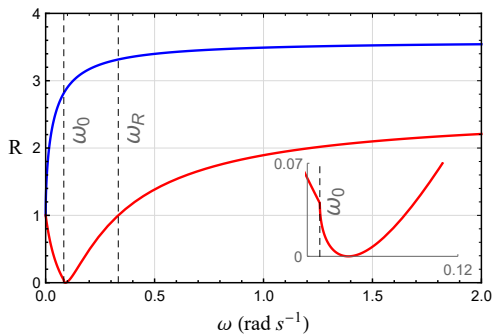


FIG. 7. Reflection coefficients R_{RCP}^- (red line) and R_{LCP}^- (blue line). R_{RCP}^- becomes greater than unit for $\omega > \omega_R$. $R_{LCP,-}$ (blue line) exhibits ubiquitous superreflectance. The inset plot highlights the behavior near the frequency ω_0 , below which $n_{RCP,-}$ has a non-null imaginary part. Here, we have used $\mu_1 = 1, n_1 = \sqrt{2}, \mu = 1, \epsilon = 3, \alpha'' = 3, b = 1 \text{ s}^{-1}$, which implies $\omega_0 = 0.1$ and $\omega_R = 1/3 \text{ s}^{-1}$.

Final remarks. In this work, we investigated the optical properties of bi-isotropic materials endowed with the anomalous Hall current of the axion electrodynamics. Four dispersive and distinct refractive indices were obtained, implying richer optical effects, such as rotatory power, Kerr rotation/ellipticity, and reflectance. Birefringence aspects were examined in terms of four rotatory power coefficients. An RP endowed with double sign reversal was reported, being a remarkable characteristic of this particular dispersive bi-isotropic media with the AHE. The first signal reversal occurs for $\omega < \omega_0$, while the second one happens for $\omega > \omega_0$, the range in which the contribution of the full $n_{RCP,-}$ index emerges, as shown in Fig. 3.

We also considered an interface separating two media: dielectric medium 1 (ϵ_1, μ_1) and bi-isotropic medium 2 with AHE (ϵ, μ, b). For normal incidence, we have written four distinct Kerr rotation angles, see Eq. (15). A continuous Kerr rotation angle (deprived of discontinuity) was found, as shown in Fig. 4, providing another key optical feature of bi-isotropic media with AHE. Such behavior occurs whenever the inequality (17) does not hold. In typical Weyl semimetals scenarios, the absence of the magnetoelectric parameter, $\alpha'' = 0$, assures the condition (17) as granted, in such a way the Kerr angle discontinuity is observed. The Kerr ellipticity was also analyzed, with its dispersive behavior illustrated in Fig. 6. The reflected wave can exhibit linear polarization ($\eta = 0$) at two distinct frequencies, left- and right-handed circular polarization ($\eta = \pm\pi/4$), and elliptical polarization (other values). Finally, the reflectance for normal incidence was also considered, starting from the Fresnel coefficients in Eq. (12). Four reflectances were carried out, with two of them depicted in Fig. 7, where an anomalous reflection behavior ($R > 1$) becomes evident at all frequencies for the blue line ($n_{LCP,-}$) and for $\omega > \omega_R$ ($n_{RCP,-}$), the exact regions where these refractive indices are negative. This effect in chiral media was recently reported in the literature for Weyl semimetals [38] when some electromagnetic parameters are negative. For the enriched bi-isotropic medium here examined, however, the anomalous reflectance can occur taking as positive all the involved parameters.

Acknowledgments. M.M.F. is supported by FAPEMA APP-12151/22, CNPq/Produtividade 311220/2019-3, and CNPq/Universal/422527/2021-1. P.D.S.S. thanks CNPq/PDJ 150584/23. We are indebted to CAPES/Finance Code 001 and FAPEMA/POS-GRAD-02575/21.

-
- [1] E. U. Condon, Theories of Optical Rotatory Power, *Rev. Mod. Phys.* **9**, 432 (1937).
 - [2] I. V. Lindell, A. H. Sihvola, S. A. Tretyakov, and A. J. Viitanen, *Electromagnetic Waves in Chiral and Bi-Isotropic Media* (Artech House, Boston, 1993).
 - [3] C.-W. Qiu, H.-Y. Yao, L.-W. Li, S. Zouhdi, and T.-S. Yeo, Routes to left-handed materials by magnetoelectric couplings, *Phys. Rev. B* **75**, 245214 (2007).
 - [4] X. Liu, J. Yang, Z. Geng, and H. Jia, Simultaneous measurement of optical rotation dispersion and absorption spectra for chiral substances, *Chirality* **8**, 32, 1071 (2022).
 - [5] Q. Zhang, E. Plum, J.-Y. Ou, H. Pi, J. Li, K. F. MacDonald, and N. I. Zheludev, Electrogyration in metamaterials: chirality and polarization rotatory power that depend on applied electric field, *Adv. Optical Mater.* **9**, 2001826 (2021).
 - [6] R. E. Newnham, *Properties of Materials - anisotropy, symmetry, structure* (Oxford University Press, New York, 2005).
 - [7] K. Shinagawa, in: *Solid-State Sciences: Magneto-Optics*, Vol. 128, Berlin: Springer-Verlag, 2000.
 - [8] K. Sato and T. Ishibashi, Fundamentals of Magneto-Optical Spectroscopy, *Front. Phys.* **10**: 946515, (2022).
 - [9] L. Ohnoutek *et. al.*, Strong interband Faraday rotation in 3D topological insulator Bi_2Se_3 , *Sci. Rep.* **6**, 19087 (2016).
 - [10] R. Shimano, G. Yumoto, J. Y. Yoo, R. Matsunaga, S. Tanabe, H. Hibino, T. Morimoto and H. Aoki, Quantum Faraday and Kerr rotations in graphene, *Nature Comm.* **4**, 1841 (2013).
 - [11] K. Sonowal, A. Singh, and A. Agarwal, Giant optical activity and Kerr effect in type-I and type-II Weyl semimetals, *Phys. Rev. B* **100**, 085436 (2019).
 - [12] W.-K. Tse and A. H. MacDonald, Giant magneto-optical Kerr effect and universal Faraday effect in thin-film topological insulators, *Phys. Rev. Lett.* **105**, 057401 (2010).
 - [13] D.E. Kharzeev, The chiral magnetic effect and anomaly-induced transport, *Prog. Part. Nucl. Phys.* **75**, 133 (2014).
 - [14] K. Fukushima, D.E. Kharzeev, and H.J. Warringa, Chiral magnetic effect, *Phys. Rev. D* **78**, 074033 (2008).
 - [15] A. A. Burkov, Chiral Anomaly and Diffusive Magneto-transport in Weyl Metals, *Phys. Rev. Lett.* **113**, 247203

- (2014).
- [16] E. V. Gorbar, V. A. Miransky, I. A. Shovkovy, and P. O. Sukhachov, *Electronic Properties of Dirac and Weyl Semimetals* (World Scientific, Singapore, 2021).
- [17] S. Kaushik, D.E. Kharzeev, and E.J. Philip, Transverse chiral magnetic photocurrent induced by linearly polarized light in symmetric Weyl semimetals, *Phys. Rev. Research* **2**, 042011(R) (2020).
- [18] K. Deng, J. S. Van Dyke, D. Minic, J. J. Heremans, and E. Barnes, Exploring self-consistency of the equations of axion electrodynamics in Weyl semimetals, *Phys. Rev. B* **104**, 075202 (2021).
- [19] E. Barnes, J. J. Heremans, and Djordje Minic, Electromagnetic Signatures of the Chiral Anomaly in Weyl Semimetals, *Phys. Rev. Lett.* **117**, 217204 (2016).
- [20] F. Wilczek, Two Applications of Axion Electrodynamics, *Phys. Rev. Lett.* **58**, 1799 (1987).
- [21] A. Sekine and K. Nomura, Axion electrodynamics in topological materials, *J. Appl. Phys.* **129**, 141101 (2021).
- [22] S.M. Carroll, G.B. Field, and R. Jackiw, Limits on a Lorentz- and parity-violating modification of electrodynamics, *Phys. Rev. D* **41**, 1231 (1990).
- [23] Z. Qiu, G. Cao and X.-G. Huang, Electrodynamics of chiral matter, *Phys. Rev. D* **95**, 036002 (2017).
- [24] P.D.S. Silva, L. Lisboa-Santos, M. M. Ferreira Jr., and M. Schreck, Effects of CPT-odd terms of dimensions three and five on electromagnetic propagation in continuous matter, *Phys. Rev. D* **104**, 116023 (2021).
- [25] A. V. Kostelevy, R. Lehnert, N. McGinnis, M. Schreck, B. Seradjeh, Lorentz violation in Dirac and Weyl semimetals, *Phys. Rev. Research* **4**, 023106 (2022).
- [26] E. Barredo-Alamilla, Daniel A. Bobylev, and Maxim A. Gorkach, Axion electrodynamics without Witten effect in metamaterials, *Phys. Rev. B* **109**, 195136 (2024).
- [27] Ming-Che Chang and Min-Fong Yang, Optical signature of topological insulators, *Phys. Rev. B* **80**, 113304 (2009).
- [28] P. D. S. Silva, M.J. Neves, M. M. Ferreira Jr., Optical properties and energy propagation in a dielectric medium supporting magnetic current, *Phys. Rev. B* **109**, 184439 (2024).
- [29] M. Stalhammar, D. Rudneva, T. H. Hansson, and F. Wilczek, Emergent Chern-Simons interactions in 3+1 dimensions, *Phys. Rev. B* **109**, 065514 (2024).
- [30] V. Shyta, J. van den Brink, and F. S. Nogueira, Chiral Meissner state in time-reversal invariant Weyl superconductors, *Phys. Rev. Research* **6**, 013240 (2024).
- [31] P. D. S. Silva, R. A. Pereira, and M. M. Ferreira Jr., Optical reflection signature of an axion dielectric with magnetic current, *Phys. Rev. B* **110**, 174427 (2024).
- [32] P. D. S. Silva and M. M. Ferreira Jr., Rotatory power reversal induced by magnetic current in bi-isotropic media, *Phys. Rev. B* **106**, 144430 (2022); Erratum, *Phys. Rev. B* **107**, 179902 (2023).
- [33] R. Gueroult, Y. Shi, J.-M. Rax, and N. J. Fisch, Determining the rotation direction in pulsars, *Nat. Commun.* **10**, 3232 (2019).
- [34] F. S. Ribeiro, P. D. S. Silva, and M. M. Ferreira Jr, Cold plasma modes in the chiral Maxwell-Carroll-Field-Jackiw electrodynamics, *Phys. Rev. D* **107**, 096018 (2023).
- [35] J.-M. Pouirol, P. Q. Liu, T. M. Slipchenko, A. Y. Nikitin, L. Martin-Moreno, J. Faist, and A. B. Kuzmenko, Electrically controlled terahertz magneto-optical phenomena in continuous and patterned graphene, *Nat. Commun.* **8**, 14626 (2017).
- [36] U. Dey, S. Nandy, and A. Taraphder, Dynamic chiral magnetic effect and anisotropic natural optical activity of tilted Weyl semimetals, *Sci. Rep.* **10**, 2699 (2020).
- [37] T. Amitani and Y. Nishida, Dynamical chiral magnetic current and instability in Weyl semimetals, *Phys. Rev. B* **107**, 014302 (2023).
- [38] Y. Nishida, Chiral Light Amplifier with Pumped Weyl Semimetals, *Phys. Rev. Lett.* **130**, 096903 (2023).
- [39] S. Konabe, Anomalous thermal radiation due to the chiral magnetic effect in Weyl semimetals, *Phys. Rev. B* **109**, 085145 (2024).
- [40] O. Trépanier, R. Duchesne, J. J. Boudreault, and R. Côté, Magneto-optical Kerr effect in Weyl semimetals with broken inversion and time-reversal symmetries, *Phys. Rev. B* **106**, 125104 (2022).
- [41] S. Ghosh, A. Sahoo, and S. Nandy, Theoretical investigations on Kerr and Faraday rotations in topological multi-Weyl semimetals, *SciPost Phys.* **15**, 133 (2023).
- [42] R. Côté, R. N. Duchesne, G. D. Duchesne, and O. Trépanier, Chiral filtration and Faraday rotation in multi-Weyl semimetals, *Results Phys.* **54**, 107064 (2023).
- [43] C. Guo, V. S. Asadchy, B. Zhao, and S. Fan, Light control with Weyl semimetals, *eLight* **3**, 2 (2023).
- [44] P. M. Valanju, R. M. Walser, and A. P. Valanju, Wave Refraction in Negative-Index Media: Always Positive and Very Inhomogeneous, *Phys. Rev. Lett.* **88**, 187401 (2002).
- [45] E. Collett, *Field Guide to Polarization*, Bellingham, Washington (USA): SPIE Press, 2005.